1995120925 N95-27346

EXTENSIONAL FLOW CONVECTING A REACTANT UNDERGOING A FIRST ORDER HOMOGENEOUS REACTION AND DIFFUSIONAL MASS TRANSFER FROM A SPHERE AT LOW TO INTERMEDIATE PECLET AND DAMKOHLER NUMBERS

N.Y. Shah and X.B. Reed, Jr.
University of Missouri-Rolla
Rolla, Missouri

S1-34
45094
P. 23

SUMMARY

Forced convective diffusion-reaction is considered for viscous axisymmetric extensional convecting velocity in the neighborhood of a sphere. For Peclet numbers in the range $0.1 \le Pe \le 500$ and for Damkohler numbers increasing with increasing Pe but in the overall range $0.02 \le Da \le 10$, average and local Sherwood numbers have been computed. By introducing the eigenfunction expansion $c(r,\theta) = \sum c_n(r)P_n(\cos\theta)$ into the forced convective diffusion equation for the concentration of a chemical species undergoing a first order homogeneous reaction and by using properties of the Legendre functions $P_n(\cos\theta)$, the variable coefficient PDE can be reduced to a system of N+1 second order ODEs for the radial functions $c_n(r)$, n=0,1,2,...,N. The adaptive grid algorithm of Pereyra and Lentini can be used to solve the corresponding 2(N+1) first order differential equations as a two-point boundary value problem on $1 \le r \le r_\infty$. Convergence of the expansion for a specific value of N can thus be established and provides "spectral" behavior as well as the full concentration field $c(r,\theta)$.

INTRODUCTION

The prevalence of small often spherical or approximately spherical particles, bubbles, or droplets in atmospheric physics, chemical reaction engineering, combustion science, and environmental technology implies the small Reynolds number (Re << 1) assumed here. For concreteness a solid sphere is also assumed. Unlike the axisymmetric uniform streaming motion past a sphere (Stokes, 1851) that is a reasonable assumption in the neighborhood of sedimenting particles or those in fluidized beds, however, the flow field in neighborhood of most particles in other natural, industrial, and laboratory circumstances is neither uniform nor can it be assumed to be the so-called slip velocity characteristic of the ensemble average over all the particles in complex, even turbulent two phase flow such as occurs in stirred tanks, for instance.

We are interested in considering other physically realistic - and therefore necessarily more complicated - flow fields that would have another domain application. The ubiquitous spherical geometry and the mathematical simplicity of axisymmetry make the axisymmetric extensional flows (Re << 1) a natural candidate. The occurence of extensional flows, in particular of locally axisymmmetric ones in the neighborhood of small spherical particles, bubbles, or drops, one of the basic building blocks in the rheology and flow of a wide variety of dispersions.

There are two axisymmetric extensional flow fields. The biaxial and uniaxial flows both have the same streamlines. However, the biaxial flow comes along the axes from $z = \pm\infty$ and approaches the poles of the sphere symmetrically, departing radially outwardly in the symmetry (x,y)-plane, whereas the uniaxial flow is oppositely directed and approaches radially symmetrically in the equatorial plane and departs along the $\pm z$ axes. Far from the sphere, the dimensionless Cartesian components of the velocity are $(\mho_x, \mho_y, \mho_z) = \pm(x, y, -2z)$, with $\pm$ referring throughout to biaxial and uniaxial, respectively.

For Re=0, all flow fields are at rest, and the Sherwood number is independent of the Peclet number and depends solely on the Damkohler number, i.e., $Sh = Sh(Da_{II})$. For Re << 1 but not identically zero, $Sh = Sh(Pe, Da_{II})$. Pe no more characterizes convection than Re characterizes the velocity field. Different velocity fields convect heat and mass differently, even if they have the same small non-zero Re and the same Pe. For Re=0, $Sh = 1 + \sqrt{Da_{II}}$, but for Re << 1, although the axisymmetric uniform streaming flow and the axisymmetric extensional flows all three have the same asymptote for Sh (viz., $1 + \sqrt{Da_{II}}$) as $Pe \to 0$, for Pe << 1 but $Pe \neq 0$, the functional dependance upon Pe, Da_{II} will be different for the uniform flow, for the biaxial flow, and for the uniaxial flow, $Sh = Sh(Pe, Da_{II})$ will be different, even though Pe and Da_{II} are identical. What is more, the local mass transfer coefficients $Sh(\theta; Pe, Da_{II})$ will be even more different. For a uniform streaming flow at infinity, Pfeffer and his co-workers have studied homogeneous first order reactions for low Reynolds number convective diffusion (Rutland and Pfeffer, 1967), (Chen and Pfeffer, 1970)

We compare and contrast the results for convective diffusion-reaction for biaxial and uniaxial flows with one another and with those for the uniform streaming flow. Our emphasis, however, is on the theoretical approach, the mathematical calculations, and the use of the Pereyra-Lentini adaptive grid algorithm, above all on certain constraints and computational limitations that arise.

THEORETICAL APPROACH

Rather than directly attacking the forced convective diffusion/diffusion-reaction equation numerically as a variable coefficient partial differential equation in which the extensional velocity field introduces the known but complicated set of variable coefficients, we take another tack. We introduce the eigenfunction expansion

$$c(r, \theta) = \sum c_n(r) \; P_n(\cos\theta) \tag{1}$$

with the $P_n(\cos\theta)$ being Legendre functions and the radial functions $c_n(r)$ are unknown. By utilizing properties of the $P_n(\mu)$, $\mu = \cos\theta$, we then reduce the single partial differential equation for $c(r,\theta)$ to a system of N+1 ordinary differential equations for the $c_n(r)$ and solve them numerically, as outlined in the next section.

The dimensionless forced convective diffusion-reaction equation investigated may be written

$$Pe \; \mho \cdot \nabla c = \nabla^2 c - Da_{II} \, c \,, \tag{2}$$

in which the second Damkohler number may be expressed in terms of the first,

$$Da_{II} = Da_I \, Pe \,, \tag{3}$$

and the Peclet number Pe for the extensional flow utilizes the characteristic velocity E a , in which E is the rate of strain at infinity and a is the radius of the solid sphere:

$$Pe = E\,a^2/\mathcal{D}\,,\; Da_I = k/E\,,\; Da_{II} = k\,a^2/\mathcal{D}\;. \tag{4}$$

The low Reynolds number axisymmetric extensional flow has two non-vanishing dimensionless velocity components

$$\begin{aligned} \mho_r &= \pm\left(r - \frac{5}{2}\,r^{-2} + \frac{3}{2}\,r^{-4} \right)\left(1 - 3\cos^2\theta \right), \\ \mho_\theta &= \pm\left(r - r^{-4}\right)\left(1 - 3\sin\theta\cos\theta \right). \end{aligned} \tag{5}$$

The ± signs refer to the biaxial/uniaxial flows, respectively. The streamlines for the two are identical and are shown in Figure 1, with the flow being oppositely directed along the streamlines. The biaxial flow comes from infinity toward the poles and exits radially symmetrically in the equatorial plane. The axisymmetric extensional creeping flow was obtained by specialization of the solution to the creeping flow equation of Batchelor (1970) for a general linear rate of strain at infinity; see also Leal (1992) for the final result.

The partial differential equation to be solved,

$$Pe\left(\mho_r(r,\theta)\,\frac{\partial c}{\partial r} + \frac{\mho_\theta(r,\theta)}{r}\,\frac{\partial c}{\partial \theta}\right) = \nabla^2 c - Pe\,Da_I\,c \tag{6}$$

may be rewritten upon introducing the expansion (1) as

$$\begin{aligned} \sum_{n=0}^{\infty}\Bigg\{ \pm\Bigg[F(r)\,\frac{dc_n}{dr}(1-3\mu^2)\,P_n(\mu) + G(r)\,c_n(r)\,(3\mu)\,(nP_n(\mu) - nP_{n-1}(\mu))\Bigg] \\ - \frac{1}{r^2}\frac{d}{dr}\left(r^2\,\frac{dc_n}{dr}\right)\,\frac{n(n+1)}{r^2}\,c_n(r) - Da_{II}\,c_n(r)\Bigg\} = 0 \end{aligned} \tag{7}$$

in which,

$$\begin{aligned} F(r) &= \left(r - \frac{5}{2}\,r^{-2} + \frac{3}{2}r^{-4} \right), \\ G(r) &= \left(1 - r^{-5}\right). \end{aligned} \tag{8}$$

In order to reduce this to a system of ordinary differential equations by utilizing the orthogonality of the $P_n(\mu)$, we must first reduce all the θ-dependent coefficients to Legendre polynomials. To accomplish this we use both algebraic and differential recurrence relations for them (Abramowitz and Stegun, 1965) , the former repeatedly as required. Ultimately, the convection terms may be written as

$$\sum_{n=0}^{\infty} \pm \left[\left(F(r)\frac{dc_n}{dr} - 3\left\{ F(r)\frac{dc_n}{dr} - nG(r)\,c_n(r) \right\} \left(\frac{1}{2n+1}\right) \right.\right.$$
$$\left.\left[\frac{(n+1)^2}{(2n+3)} + \frac{n^2}{(2n-1)}\right] - 3\,\frac{n^2}{(2n-1)} G(r)\,c_n(r) \right) P_n(\mu) \tag{9}$$
$$-3\left\{ F(r)\frac{dc_n}{dr} - nG(r)\,c_n(r) \right\} \left\{ \frac{(n+1)(n+2)}{(2n+1)(2n+3)} \; P_{n+2}(\mu) \right.$$
$$\left. + \frac{n(n-1)}{(2n-1)} \left[\frac{1}{(2n+1)} + G(r)\,c_n(r)\right] P_{n-2}(\mu) \right\}$$

The remaining terms of the equation need not be rewritten. Upon utilizing the orthogonality of the $P_n(\mu)$ and solving for the second derivatives, we obtain for the general n ($n \neq 0,1$),

$$\frac{d^2 c_n}{dr^2} = \pm\, Pe \left[F(r)\frac{dc_n}{dr} - \frac{3}{(2n+1)} \left(\frac{(k+1)^2}{(2n+3)} + \frac{n^2}{(2n-1)} \right) \right.$$
$$-3\,\frac{n(n-1)}{(2n-1)(2n-3)} \left(F(r)\frac{dc_{n-2}}{dr} - (n-2)\,G(r)\,c_{n-2}(r) \right) \tag{10}$$
$$\left. -3\,\frac{(n+1)(n+2)}{(2n+3)(2n+5)} \left(F(r)\frac{dc_{n+2}}{dr} + (n+3)\,G(r)\,c_{n+2}(r) \right) \right]$$
$$-\frac{2}{r}\frac{dc_n}{dr} + \frac{n(n+1)}{r^2} c_n(r) + Da_{II}\; c_n(r)$$

In the computations and results, it is more informative to vary Pe and Da_I (called K in the program and figures).

The boundary conditions on $c(r,\theta)$ are

$$\begin{aligned} c(r,\theta) &= 1\ , \\ c(r \to \infty, \theta) &= 0\ , \end{aligned} \tag{11}$$

which imply

$$\begin{aligned} c_0(r=1) &= 1, \\ c_n(r=1) &= 0, \quad n \geq 1, \\ c_n(r \to \infty) &= 0, \quad n \geq 0. \end{aligned} \tag{12}$$

NUMERICAL ALGORITHM

The algorithm of Pereyra and Lentini (1978) as codified now in the IMSL subroutine DBVPFD was used. It is a robust program for solving two-point boundary value problems. In order to solve the ordinary differential equation system represented by (10)-(12), we first must terminate the infinite series (1) at $N < \infty$, and the spatial domain at $r_\infty < \infty$. The former leads to a finite system of second order equations for which $c_n(r) \equiv 0$ for $n < 0$, $n > N$. The latter leads to the modified boundary conditions

$$\begin{aligned} c_0(r=1) &= 1 \\ c_n(r=1) &= 0\ , \quad n \geq 0 \\ c_n(r=r_\infty) &= 0\ , \quad n \geq 0\ . \end{aligned} \tag{13}$$

The results for $c_n\,(r;Pe,Da_I)$ will obviously depend upon N and r_∞. The latter (r_∞) is a parameter that can be varied in the program. The former (N) must be selected before the program can be run, but once selected (as conservatively as possible), convergence of the series can be established. The other crucial computational parameters in the subroutine are the initial and maximum number of mesh points (NINIT, MXGRID).

Finally, the system of N+1 second order equations must be converted in the usual way to a system of 2(N+1) first order equations in order to employ the IMSL subroutine:

$$\begin{aligned}
c_0(r) &\rightarrow y_1(x) \\
c_1(r) &\rightarrow y_2(x) \\
&\ \vdots \\
c_{N-1}(r) &\rightarrow y_{\frac{NEQNS}{2}-1}(x) \\
c_N(r) &\rightarrow y_{\frac{NEQNS}{2}}(x) \\
\frac{dc_0}{dr}(r) &= \frac{dy_1}{dx}(x) \rightarrow y_{\frac{NEQNS}{2}+1}(x) \\
\frac{dc_1}{dr}(r) &= \frac{dy_2}{dx}(x) \rightarrow y_{\frac{NEQNS}{2}+2}(x) \\
&\ \vdots \\
\frac{dc_n}{dr}(r) &= \frac{dy_{n+1}}{dx}(x) \rightarrow y_{\frac{NEQNS}{2}+n+1}(x) \\
&\ \vdots \\
\frac{dc_{N-1}}{dr}(r) &= \frac{dy_{\frac{NEQNS}{2}-1}}{dx}(x) \rightarrow y_{NEQNS-1}(x) \\
\frac{dc_N}{dr}(r) &= \frac{dy_{\frac{NEQNS}{2}}}{dx}(x) \rightarrow y_{NEQNS}(x)
\end{aligned} \tag{14}$$

RESULTS AND DISCUSSION

For a practicing engineer and for many engineering and other scientists and mathematicians, the principal goal of such an investigation would be a relation between the average Sherwood number (the dimensionless mass transfer coefficient) Sh and the physicochemical parameters, viz., Sh(Pe;Da_I). Of some practical interest is also the local Sherwood number, which for an axisymmetric convecting velocity would be expressible as Sh(θ;Pe,Da_I), the integral of which, when carried out over the surface of the sphere, yields the average Sherwood number Sh. The magnitude of the local Sherwood number is the normal derivative of the concentration field c(r,θ) at the sphere surface, $\partial c/\partial r\,(r,\theta)|_{r=1}$. Although the concentration field c(r,θ) in other approaches to the forced convective diffusion-reaction problem would be the object of the numerical research, it generally receives short schrift as being of little practical interest. In multiparticle systems, the extent of the concentration fields non-negligible level for a single particle can for instance, be useful in assessing, or at least estimating, the minimum interparticle distance at which concentration fields of neighboring particles would affect one another.

We start our discussion, neither with Sh(θ;Pe,Da_I) nor with c(θ;Pe,Da_I), but with the object of our numerical study, the radial functions c_n(r;Pe,Da_I), denoted as c_n(r;Pe,K). In Figure 2a,b for r_∞ (≡R in the notation employed throughout the paper) = 10 and Pe=5, K=1 we show the radial functions c_n(r), for n=0,1,2,...,70 for a biaxial flow. Consistent with the reflection symmetry across the equatorial ($\theta=\pi/2$) plane, only the even radial modes are nonvanishing. The radial functions decrease in magnitude, and N=70 clearly produces a convergent series.

Biaxial

When the radial functions are multiplied respectively by their corresponding Legendre polynomials, the isocontour plot shown in the upper half of Figure 1 results. The biaxial velocity field produces the thin(ner) stagnation concentration boundary layer at the poles. The concentration wake then imbeds the equatorial plane symmetrically. There are, to emphasize the point, neither momentum boundary layers nor momentum wakes (Re << 1). At the same Pe, r_∞, and N, an increase of K from 1 to 2 reduces (Figure 3) the boundary layer a bit and the wake more, effects that are still more pronounced for K=5 (Pe=5) in Figure 4. For K=10 (Pe=5), all of the isocontours (0.1-0.9 in increments of 0.1) except for c=0.01 are spherically symmetric (Figure5), as far as is apparent to the naked eye (and undoubtedly a boon to theoreticians).

For an increase of Pe to 50, the K=2 (Figure 6) is of course dissimilar to that for Pe=5, but for K=5,10 similar remarks apply to the Pe=50 isocontours: there is one nonspherical isocontour for K=5 and none at K=10 (Plots not shown).

For a further increase to Pe=200 (Figure 7) the isocontours show a 2-d salient at K=1, which has become almost spherically symmetric at K=2 (Figure 8). For K=5 and 10 (Plots not shown) spherical symmetry reigns, the differences being solely the decreasing radii of the circles with increasing K.

The isocontour plot for Pe=500 and K=0.5 (Figure 9) is similar to that for Pe=200 and K=1 (Figure 7).

Uniaxial

The area of stagnation concentration boundary layer for uniaxial extensional creeping flow is centered on the stagnation velocity ring, the equator. The concentration wakes are two, stretching from the poles ($\theta=0,\pi$), qualitatively similar to the concentration wake on the downwind pole of a sphere in a uniform streaming flow at infinity. Such observations are rendered more faithfully in Figure 10 for Pe=5, K=5 than in words.

An increase from K=5 to 10 for the same Peclet number (Pe=5) brings about expected isocontours (Figure 11), as does an increase of Pe to 50 for K=5 (Figure 12) and for K=10 (Figure 13), by which values spherical isocontours result.

Local Sherwood Numbers

For fast reactions (Da_I=K=5,10), spherical isocontours were observed. An increase in the convection (i.e., in Pe) served to feed the reaction faster but did not further influence the spherical symmetry of the isocontours, once a Pe was reached at which they were spherical. This is nowhere more evident than for the biaxial flow in Figures 14a,b for K=5 and 10 respectively; Pe=5, 50, 200, 500. There are slight local maxima at $\theta=0,\pi$ and a slight local minimum at $\theta=\pi/2$. Increases in Pe lead to dramatic increases in the level of mass transfer rates without however appreciably affecting local values over the surface, relative to one another. The increase in Da_I from 5 to 10 increases the level of order 10 % for each Pe shown.

Absent reaction, biaxial convective diffusion produces a local Sherwood number that is peaked at $\theta=0,\pi$ and troughed around $\theta=\pi/2$. The clear minimum is reduced rapidly as the maxima increase with K (Figure 15a, Pe=5; Figure 15b, Pe=50; Figure 15c, Pe=200; Figure 15d, Pe=500).

For a uniaxial flow the convective diffusion problem without reaction produces a pronounced maximum at $\theta=\pi/2$ and minima at $\theta=0,\pi$, as expected (Figure 16a). Also as expected, the strong maximum is reduced relative to the minima with increasingly fast reaction (Figure 16a), an effect observed with higher Pe (Figure 16b,c).

Crossplots for K=5 and 10 for the several values of Pe in Figures 17a,b, emphasizing the weak θ-dependence of $Sh(\theta)$ for fast reactions.

Average Sherwood Number

Different velocity fields convect heat and mass differently, as is evident even for the two types of axisymmetric extensional flows. Concentration isocontours, other than those for very high Da_I, are different for biaxial and uniaxial flows.

For Pe=5, convective diffusion (K=0 in Tables 1,2) by uniaxial flow manifests a greater average mass transfer coefficient than by biaxial flow. Indeed, strictly speaking, for any value of Pe and K, $Sh(Pe_i, K_j)_{uni} > Sh(Pe_i, K_j)_{bi}$, as is evident from Tables 1 and 2.

Nonetheless, for Pe=5, K=1, Sh_{uni} is greater than Sh_{bi} by only 0.07; for K=2, by only 0.03; for K=5, by only 0.005. For Pe=50 and K=5, 10, $Sh_{uni} > Sh_{bi}$ only in the third decimal place, which also holds for the same K's, at Pe=200. For K=10, at Pe=500, they differ only in the fourth decimal place. Thus, from this limited set of results, Sh is virtually identical for uniaxial and biaxial flows for K=5,10 for $Pe \geq 50$. For smaller reaction rates and for smaller convection (smaller Pe), small but perceptible differences will arise between biaxial and uniaxial creeping flows, with the latter being the larger of the two.

BIBLIOGRAPHY

1. Stokes, G.G.: On the Effect of Internal Friction of Fluids on the Motion of Pendulums. Trans. Cambridge Phil. Soc., vol. 9, Part II, 1851, pp 8-106.
2. Rutland, L.; and Pfeffer, R.: Mass Transfer from a Single Sphere in Stokes' Flow with a Homogeneous Chemical Reaction. A.I.Ch.E. J., vol. 13, no. 1, Jan. 1967, pp 182-186.
3. Chen, W.C.; and Pfeffer, R.: Local and Over-All Mass Transfer Rates around Solid Spheres with

First-Order Homogeneous Chemical Reaction. Ind. Eng. Chem. Fundamentals, vol. 9, no. 1, Feb. 1970, pp 101-107.
4. Batchelor, G.K.: An Introduction to Fluid Dynamics. Cambridge, 1970
5. Leal, L.G.: Laminar Flow and Convective Transport Processes. Butterworth, 1992
6. Abramowitz, M.; and Stegun, I.A.: Handbook of Mathematical Functions. Dover 1965
7. Pereyra, Victor (1978), PASVA3: An adaptive finite-difference FORTRAN program for first order nonlinear boundary value problems, in Lecture Notes in Computer Science, 76, Springer-Verlag, Berlin, 67-88.

ACKNOWLEDGEMENTS

Computer runs for small values of Pe were run on the HP 9000 worksatations in the Computer Center of the University of Missouri - Rolla; the Director, David Dearth, and several of his colleagues have been helpful, but Gerry O'Brennan deserves special credit. Because of the local hardware limitations, we are especially indebted to John Gee and CRAY Research for access to EL92, with sufficient memory to run the larger memory and CPU intensive (higher Pe, N) jobs. Without the Mr. Gee's generous cooperation, we would not have been able to run Pe ≥ 50.

FIGURE 1

CONCENTRATION ISOCONTOURS

BIAXIAL FLOW WITH HOMOGENEOUS REACTION

PE=5 K=1 R=10 ORDER=1 L=70

LEVELS: 0.01, 0.1 TO 0.9 BY 0.1

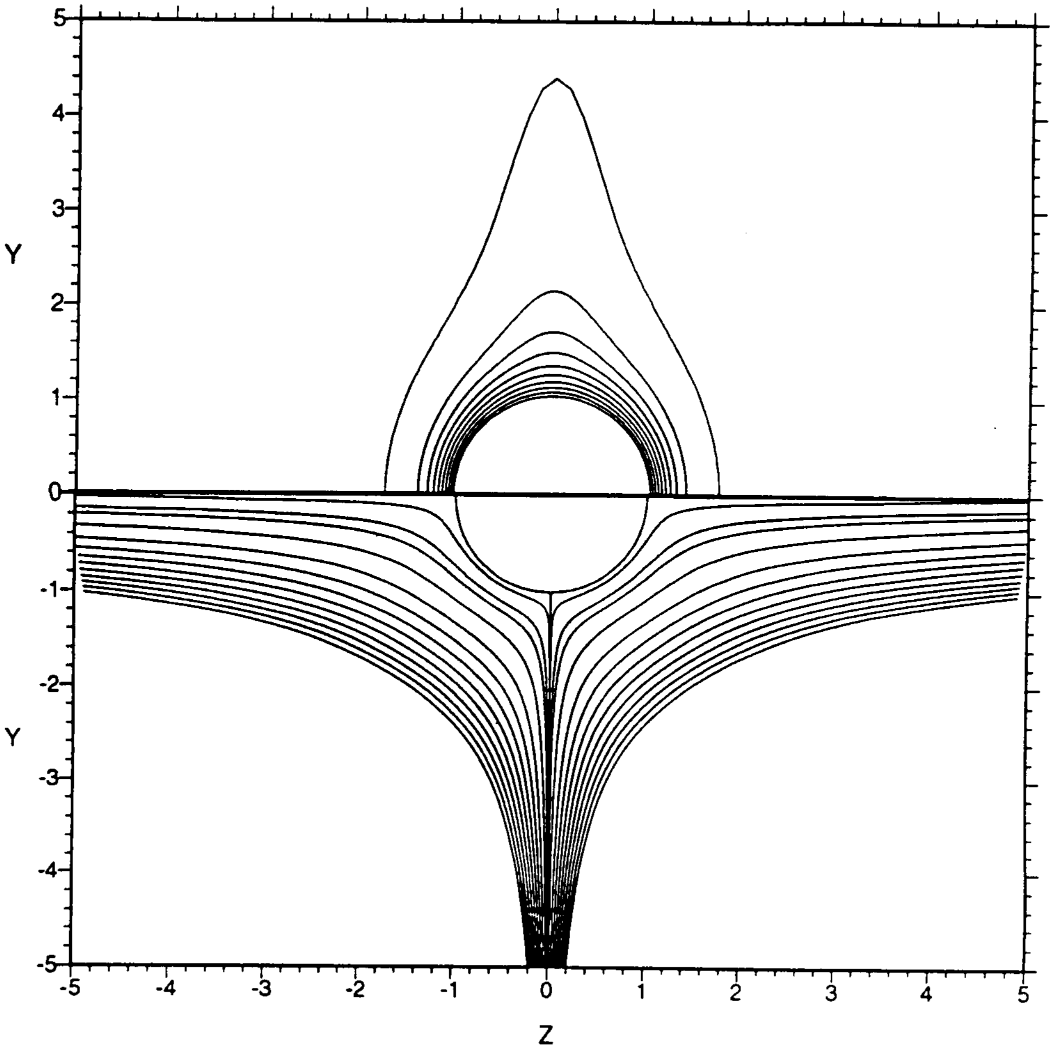

STREAM FUNCTION ISOCONTOURS

BIAXIAL AND UNIAXIAL EXTENSIONAL FLOW

LEVELS: +/- 0.01, +/- 0.1, -5 TO 5 BY 0.5

FIGURE 2a

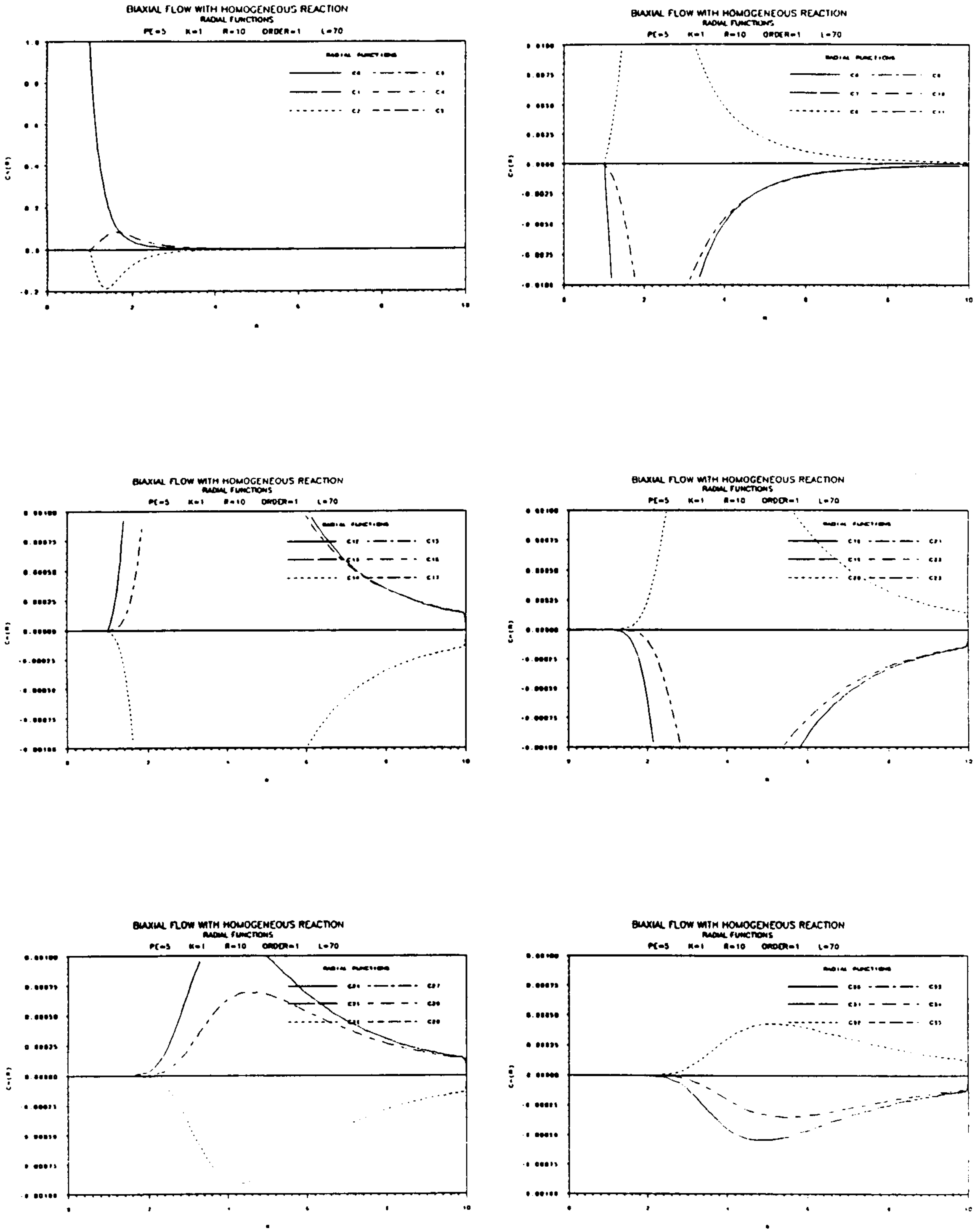
BIAXIAL FLOW WITH HOMOGENEOUS REACTION
RADIAL FUNCTIONS
PE=5 K=1 R=10 ORDER=1 L=70

FIGURE 2b

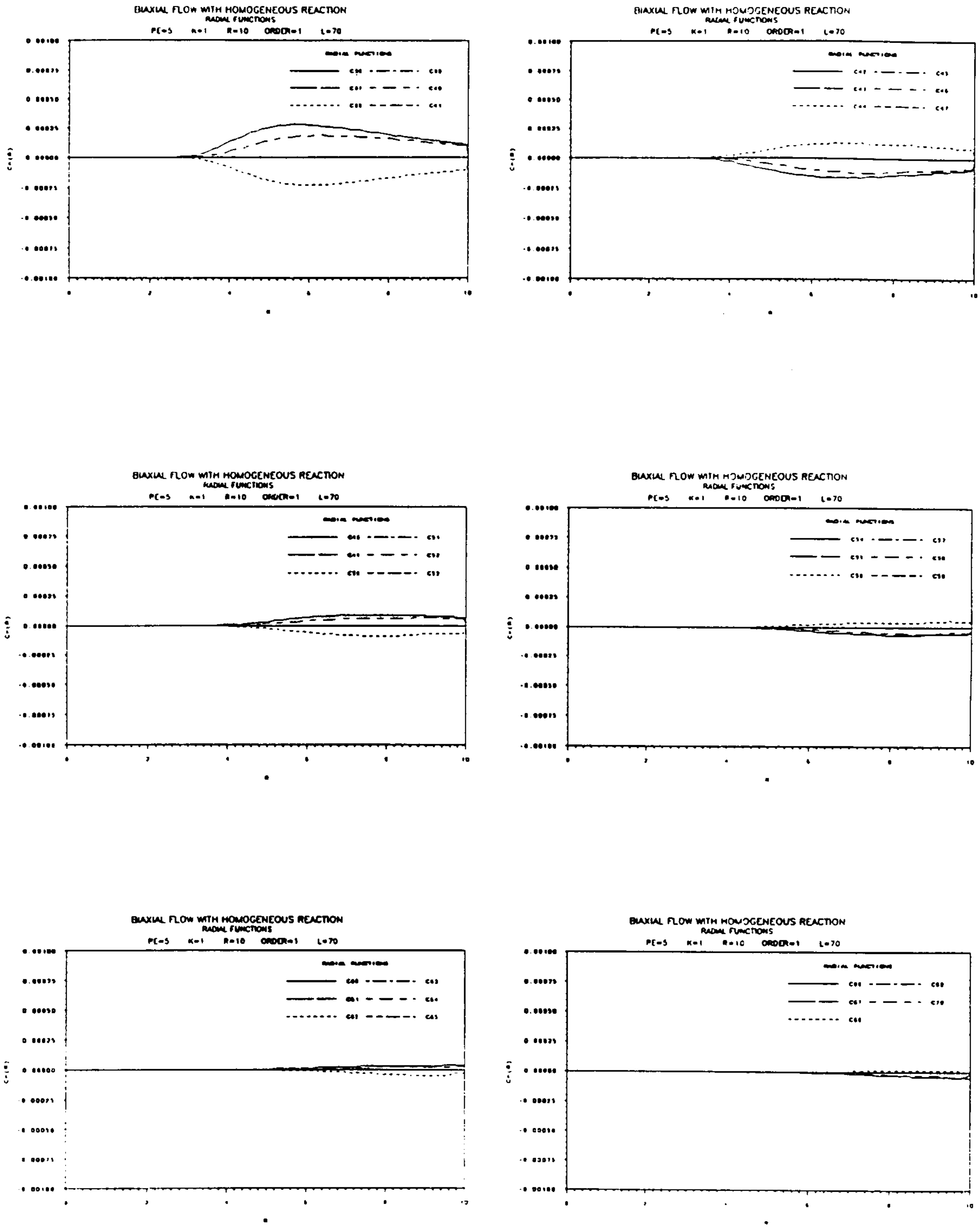
BIAXIAL FLOW WITH HOMOGENEOUS REACTION
RADIAL FUNCTIONS
PE=5 K=1 R=10 ORDER=1 L=70
BIAXIAL FLOW WITH HOMOGENEOUS REACTION
RADIAL FUNCTIONS
PE=5 K=1 R=10 ORDER=1 L=70
BIAXIAL FLOW WITH HOMOGENEOUS REACTION
RADIAL FUNCTIONS
PE=5 K=1 R=10 ORDER=1 L=70
BIAXIAL FLOW WITH HOMOGENEOUS REACTION
RADIAL FUNCTIONS
PE=5 K=1 R=10 ORDER=1 L=70
BIAXIAL FLOW WITH HOMOGENEOUS REACTION
RADIAL FUNCTIONS
PE=5 K=1 R=10 ORDER=1 L=70
BIAXIAL FLOW WITH HOMOGENEOUS REACTION
RADIAL FUNCTIONS
PE=5 K=1 R=10 ORDER=1 L=70

FIGURE 3

CONCENTRATION ISOCONTOURS

BIAXIAL FLOW WITH HOMOGENEOUS REACTION

PE=5.00 K=2.00 R=10.0 ORDER=1 L=70

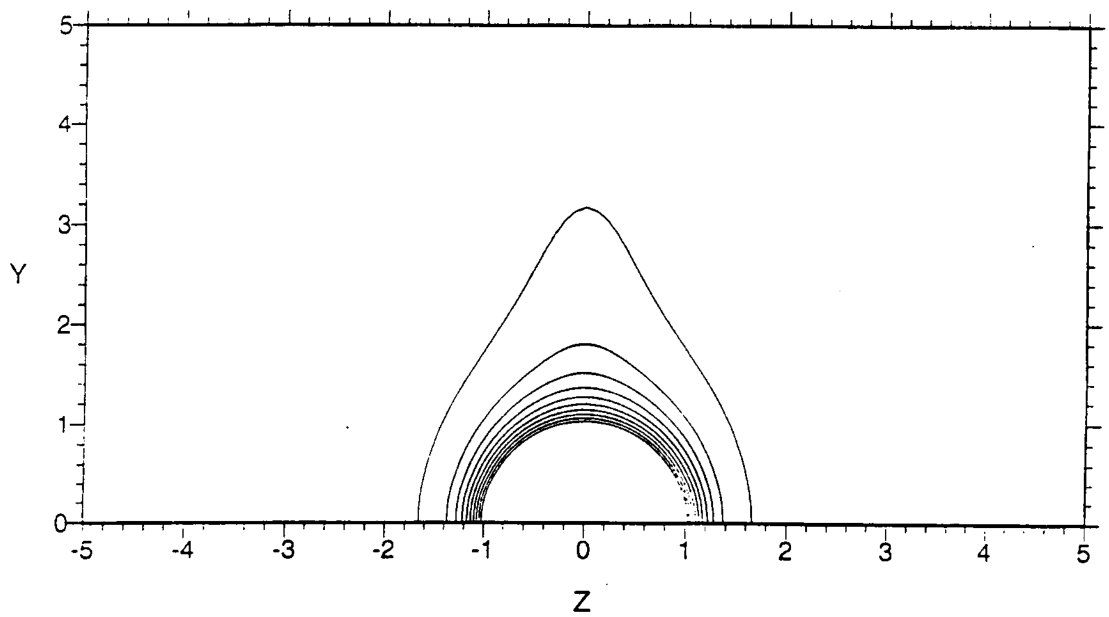

FIGURE 4

CONCENTRATION ISOCONTOURS

BIAXIAL FLOW WITH HOMOGENEOUS REACTION

PE=5.00 K=5.00 R=10.0 ORDER=1 L=70

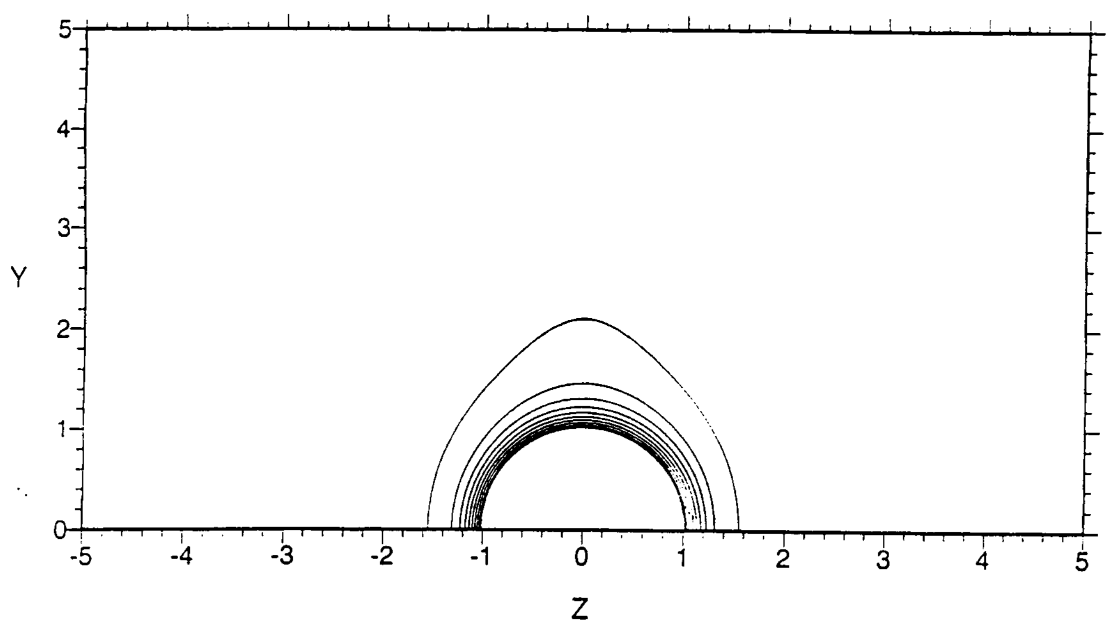

FIGURE 5
CONCENTRATION ISOCONTOURS
BIAXIAL FLOW WITH HOMOGENEOUS REACTION
PE=5.00 K=10.00 R=10.0 ORDER=1 L=70

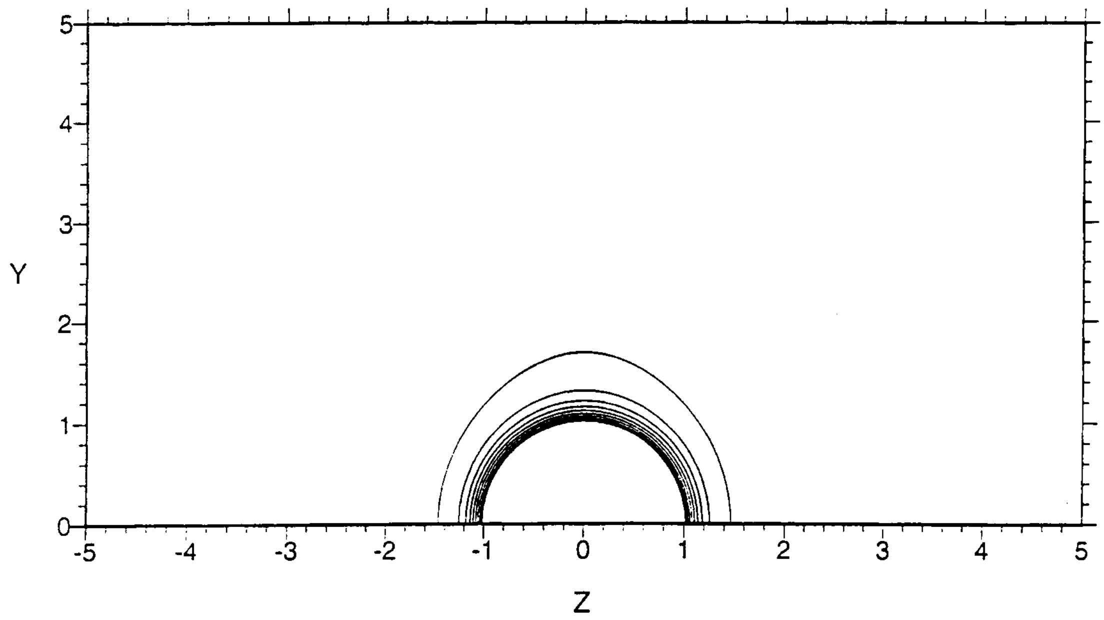

FIGURE 6
CONCENTRATION ISOCONTOURS
BIAXIAL FLOW WITH HOMOGENEOUS REACTION
PE=50.00 K=2.00 R=5.0 ORDER=1 L=70

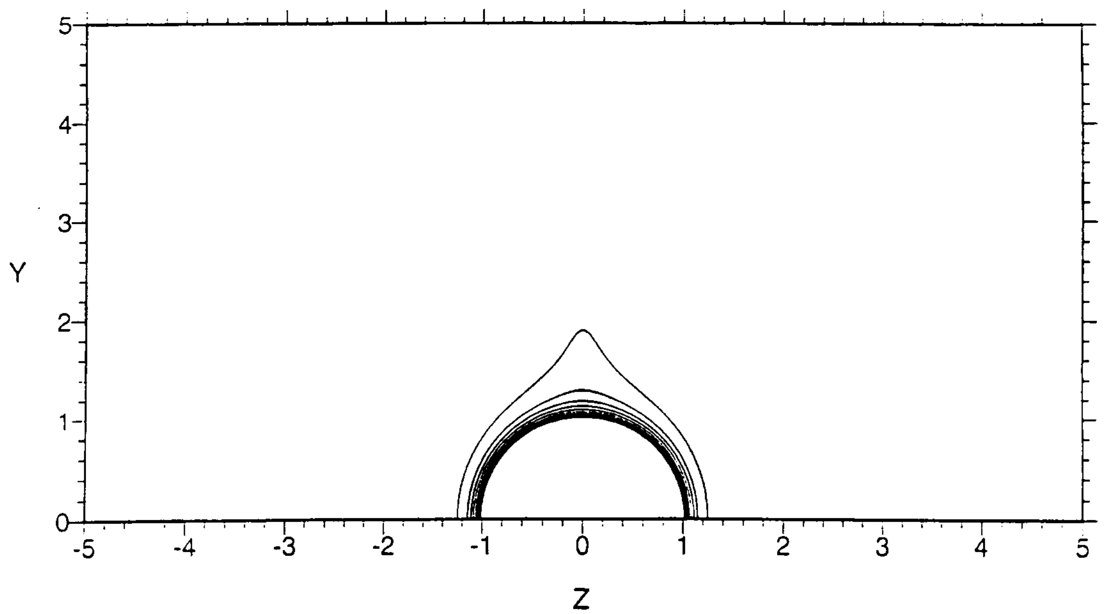

FIGURE 7

CONCENTRATION ISOCONTOURS

BIAXIAL FLOW WITH HOMOGENEOUS REACTION

PE=200.00 K=1.00 R=5.0 ORDER=1 L=70

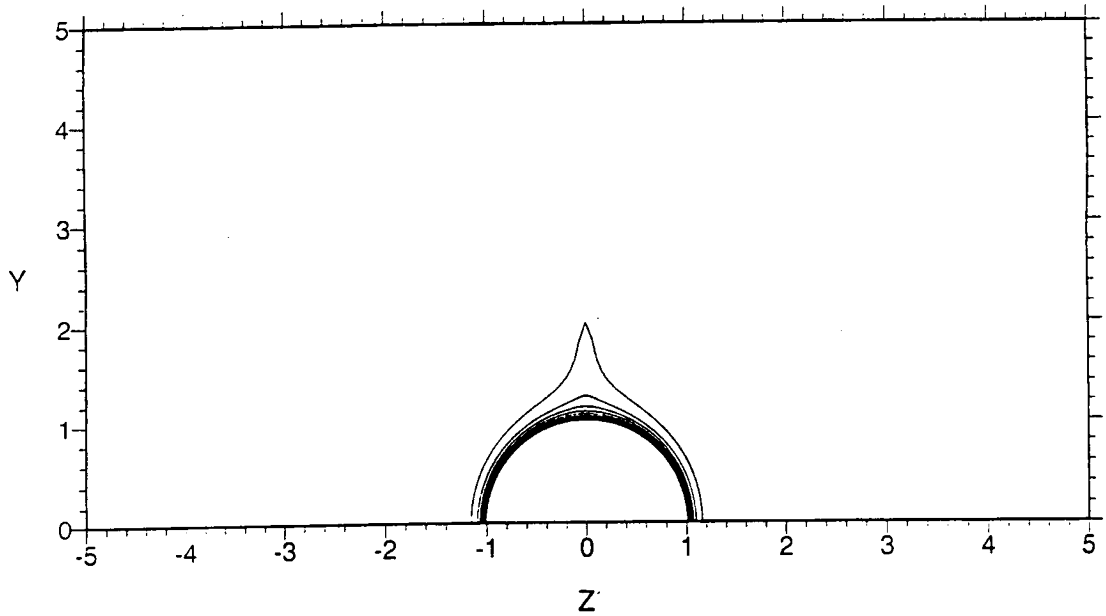

FIGURE 8

CONCENTRATION ISOCONTOURS

BIAXIAL FLOW WITH HOMOGENEOUS REACTION

PE=200.00 K=2.00 R=5.0 ORDER=1 L=70

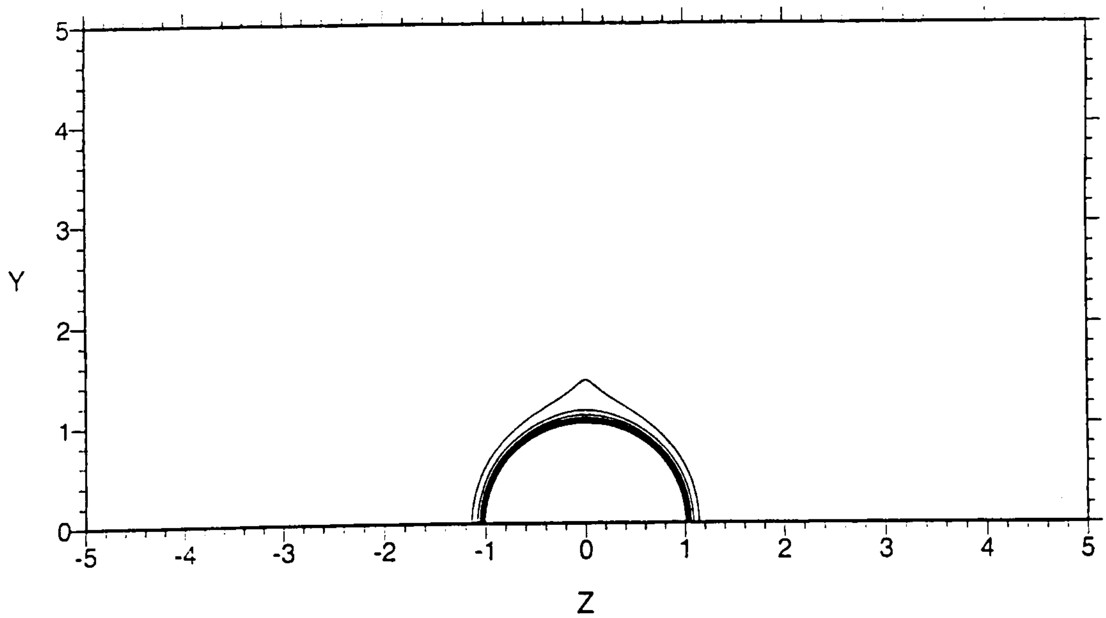

FIGURE 9

CONCENTRATION ISOCONTOURS

BIAXIAL FLOW WITH HOMOGENEOUS REACTION

PE=500.00 K=0.50 R=5.0 ORDER=1 L=70

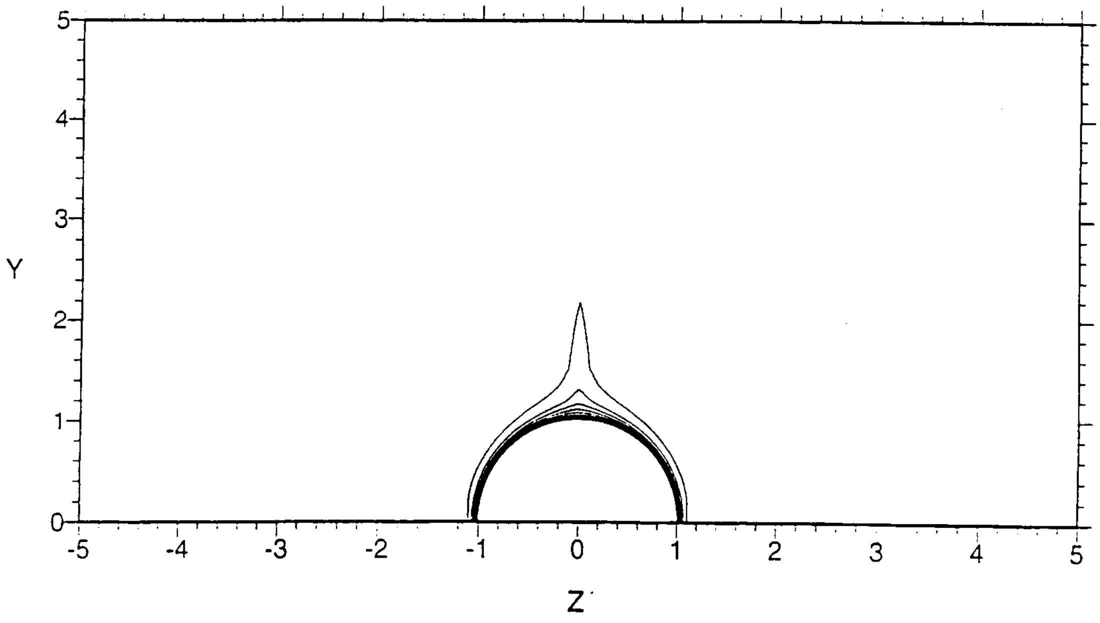

FIGURE 10

CONCENTRATION ISOCONTOURS

UNIAXIAL FLOW WITH HOMOGENEOUS REACTION

PE=5.00 K=5.00 R=10.0 ORDER=1 L=70

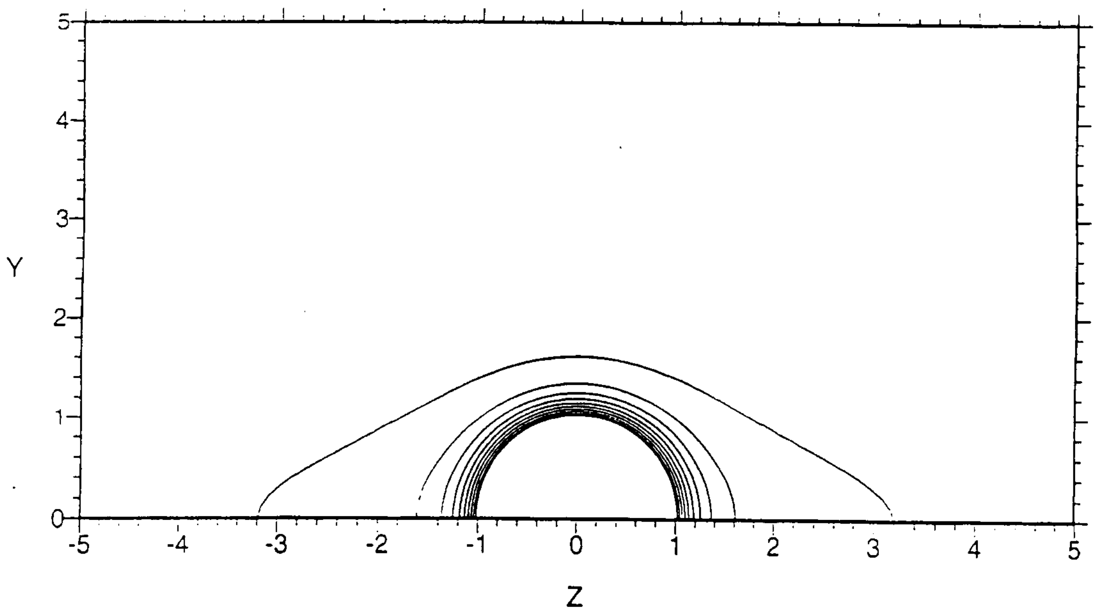

FIGURE 11

CONCENTRATION ISOCONTOURS

UNIAXIAL FLOW WITH HOMOGENEOUS REACTION

PE=5.00 K=10.00 R=10.0 ORDER=1 L=70

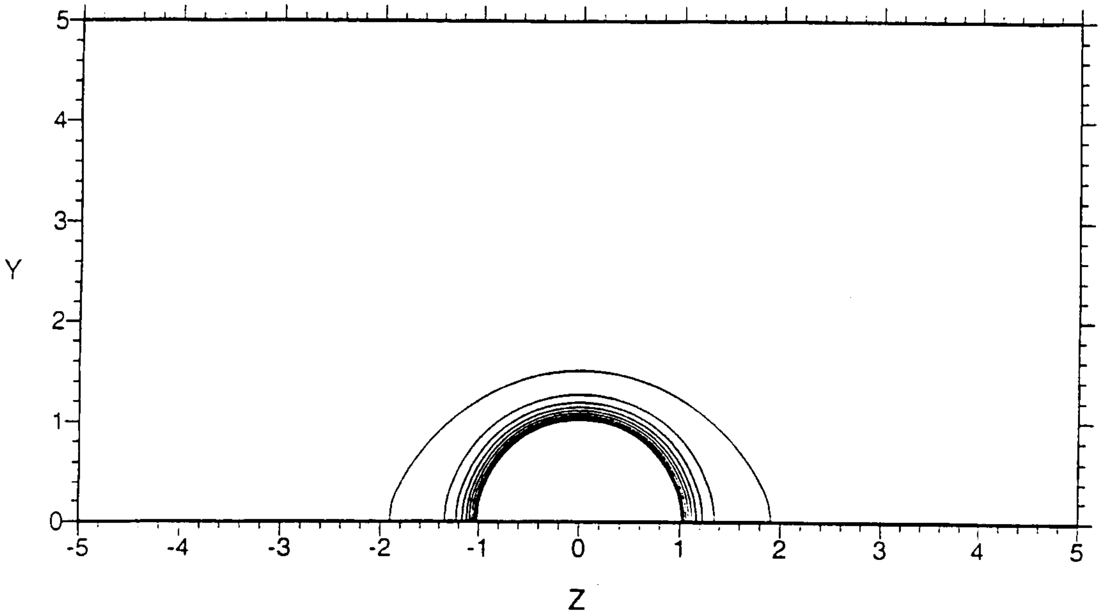

FIGURE 12

CONCENTRATION ISOCONTOURS

UNIAXIAL FLOW WITH HOMOGENEOUS REACTION

PE=50.00 K=5.00 R=5.0 ORDER=1 L=70

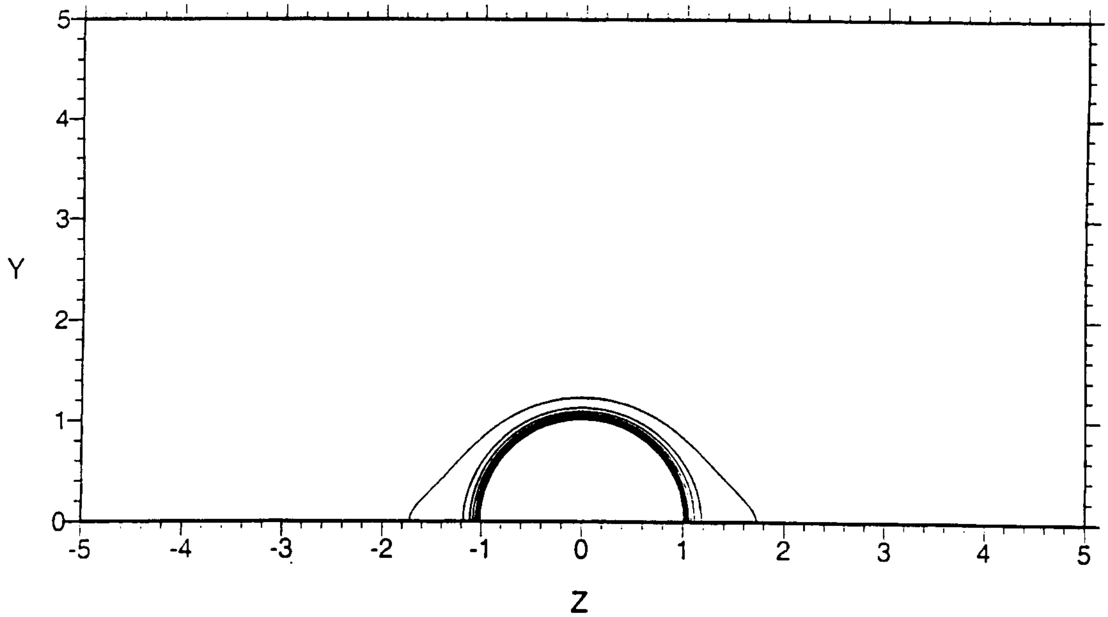

FIGURE 13

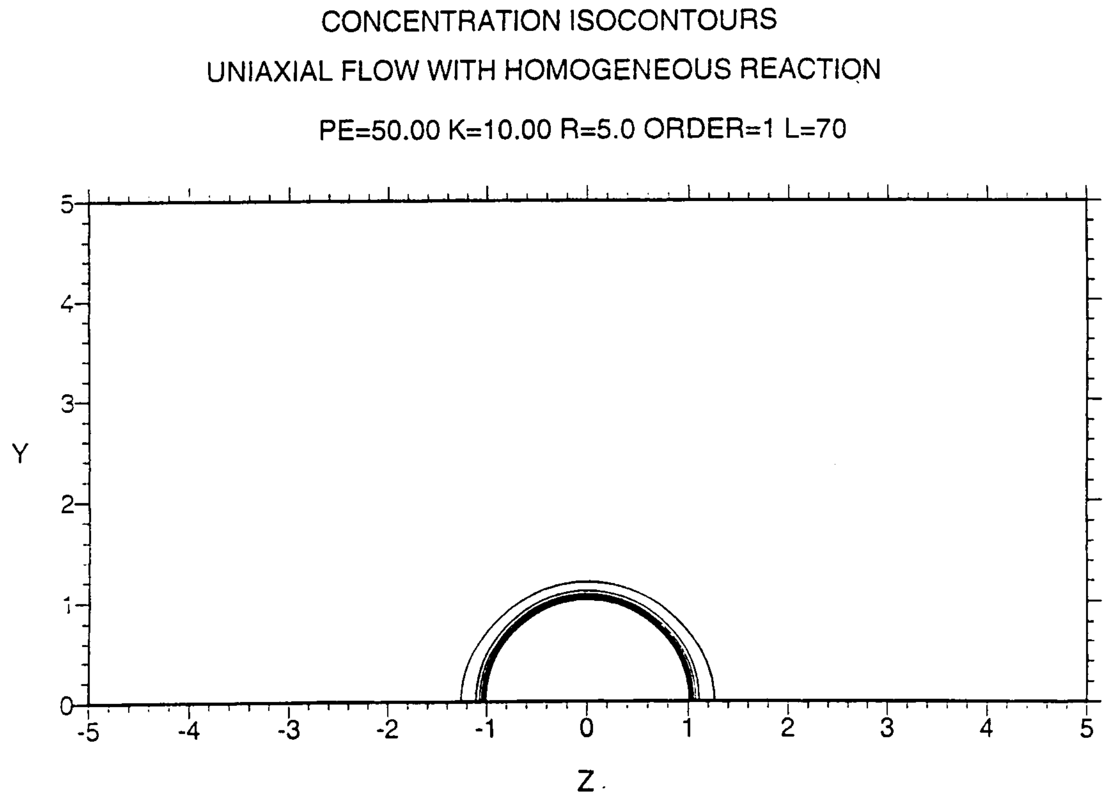

FIGURE 14a

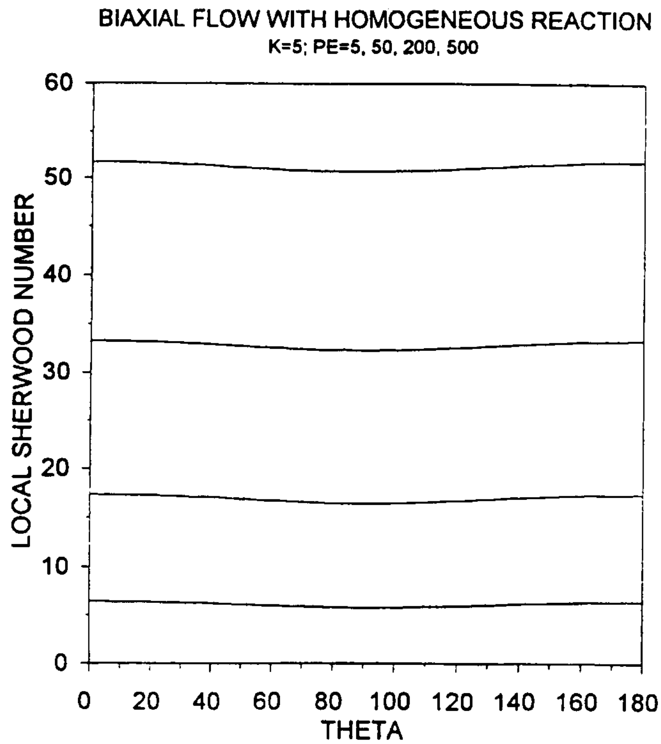

FIGURE 14b

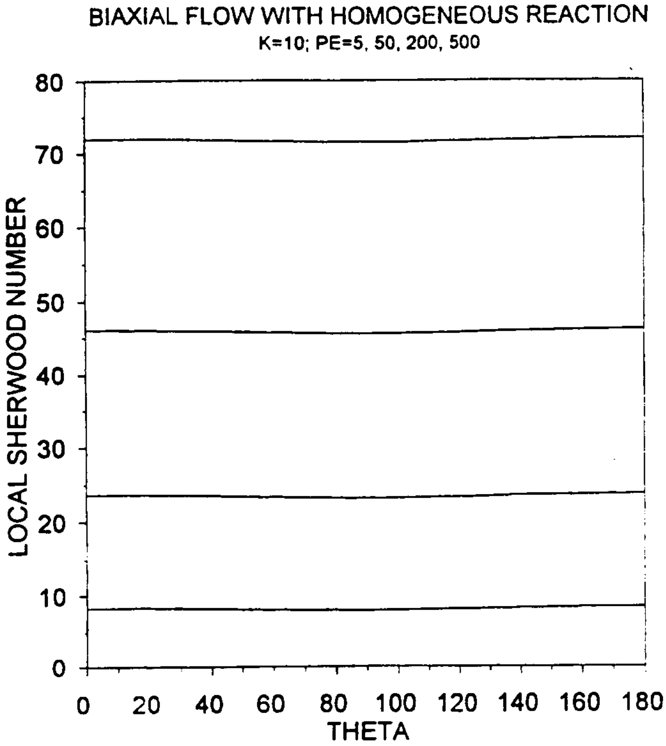

FIGURE 15a

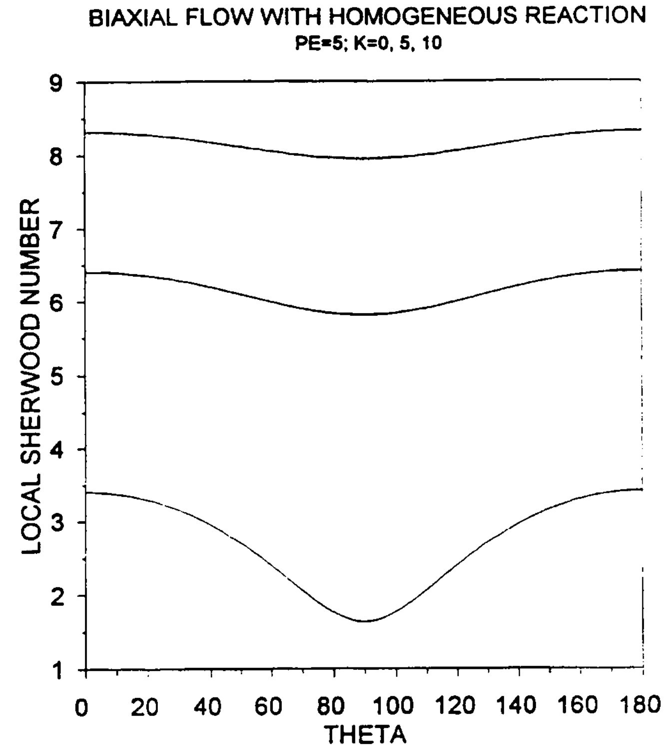

FIGURE 15b

BIAXIAL FLOW WITH HOMOGENEOUS REACTION

PE=50; K= 5, 10

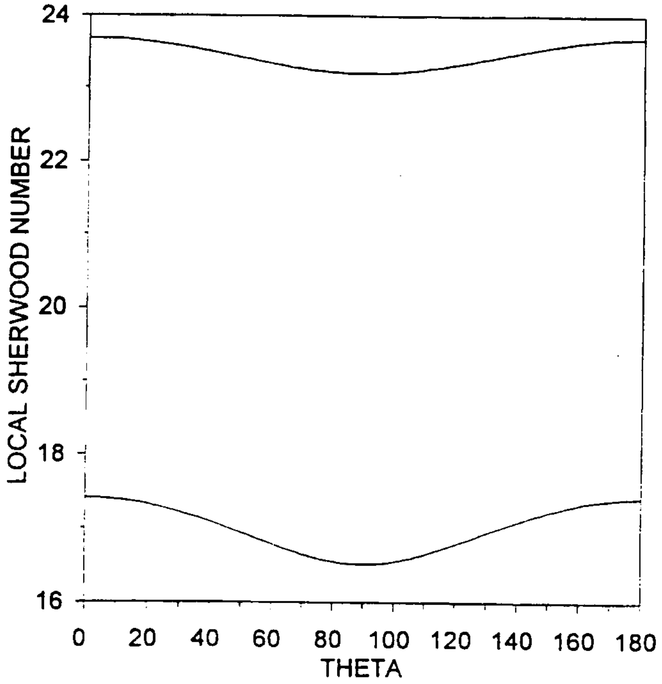

FIGURE 15c

BIAXIAL FLOW WITH HOMOGENEOUS REACTION

PE=200; K= 5, 10

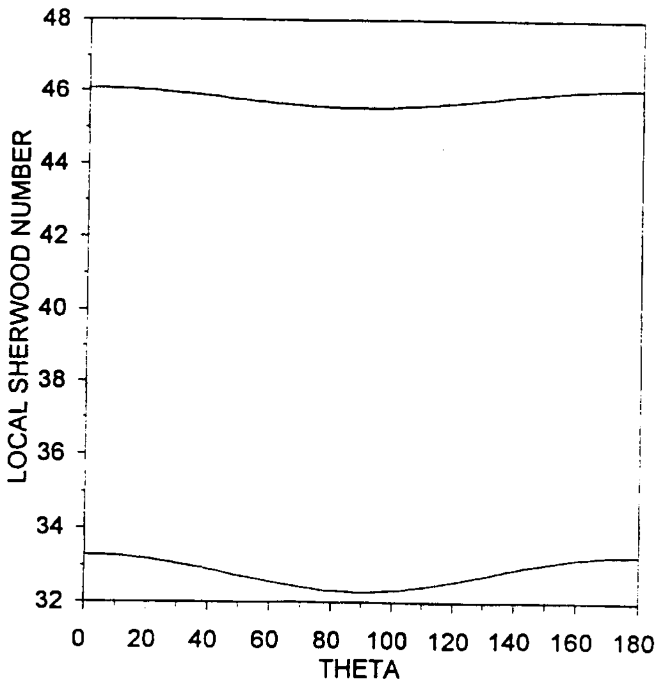

FIGURE 15d

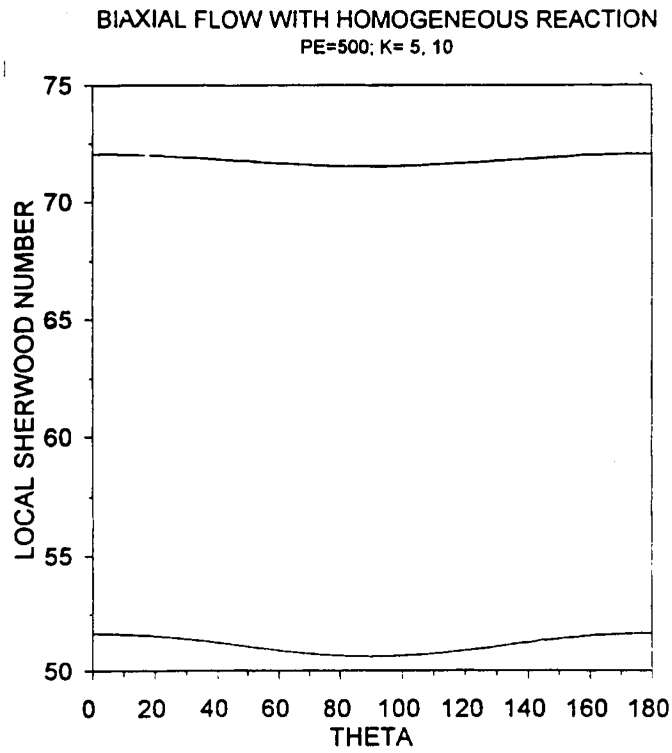

FIGURE 16a

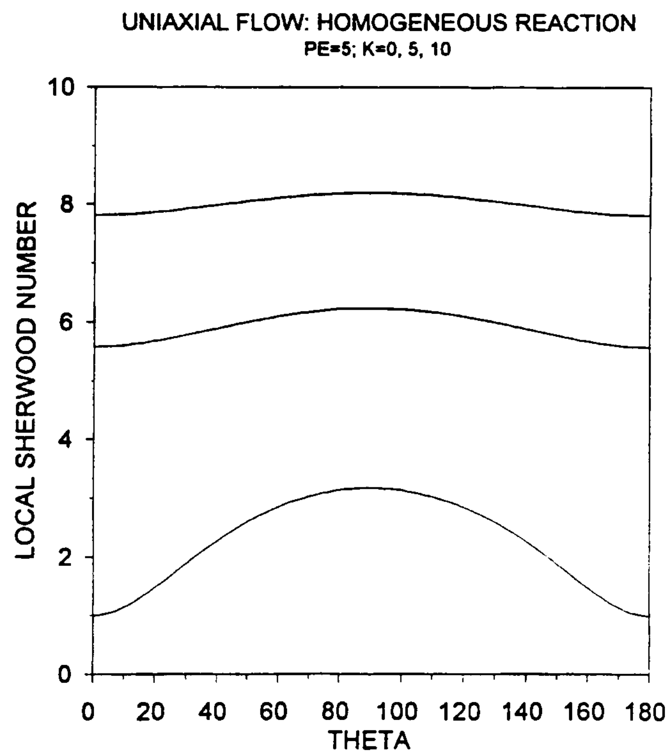

FIGURE 16b

UNIAXIAL FLOW: HOMOGENEOUS REACTION

PE=50; K= 5, 10

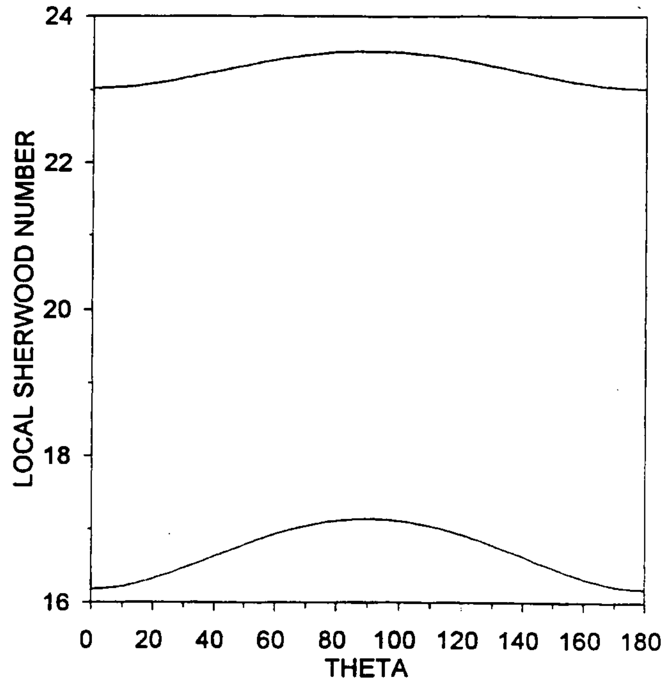

FIGURE 16c

UNIAXIAL FLOW: HOMOGENEOUS REACTION

PE=200; K= 5, 10

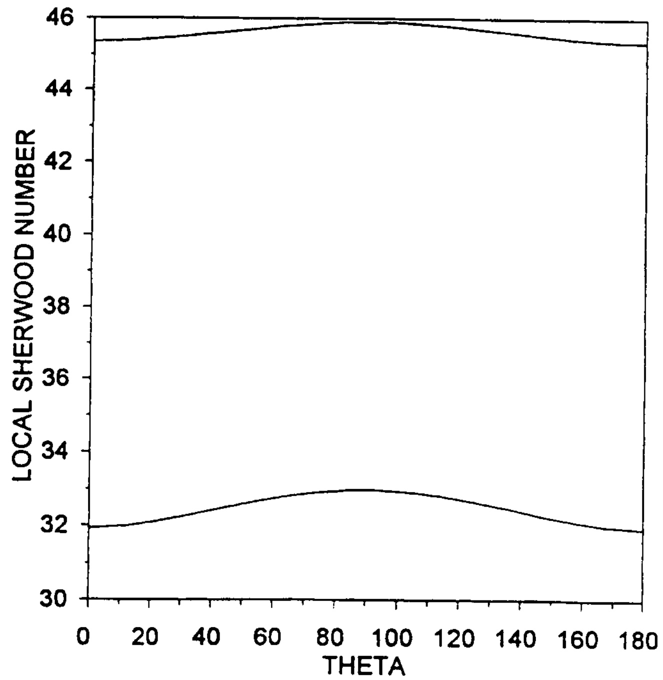

FIGURE 17a

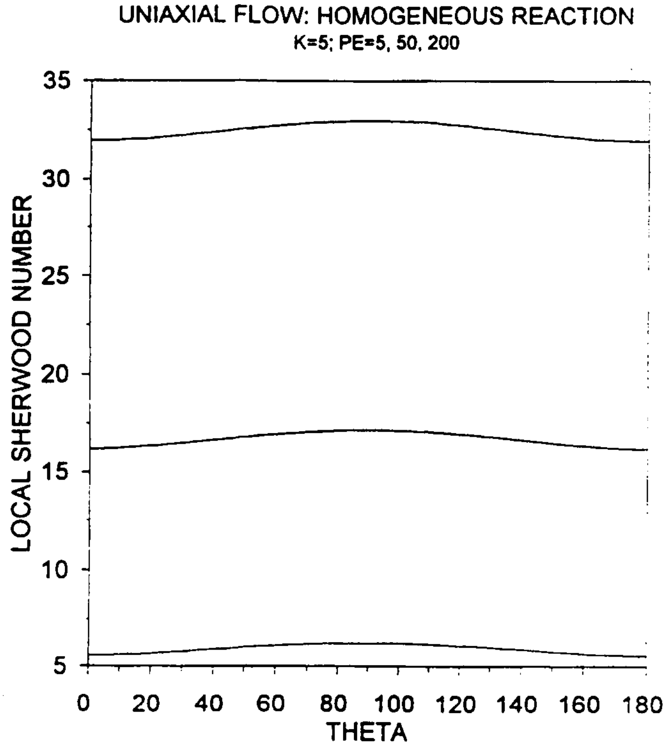

FIGURE 17b

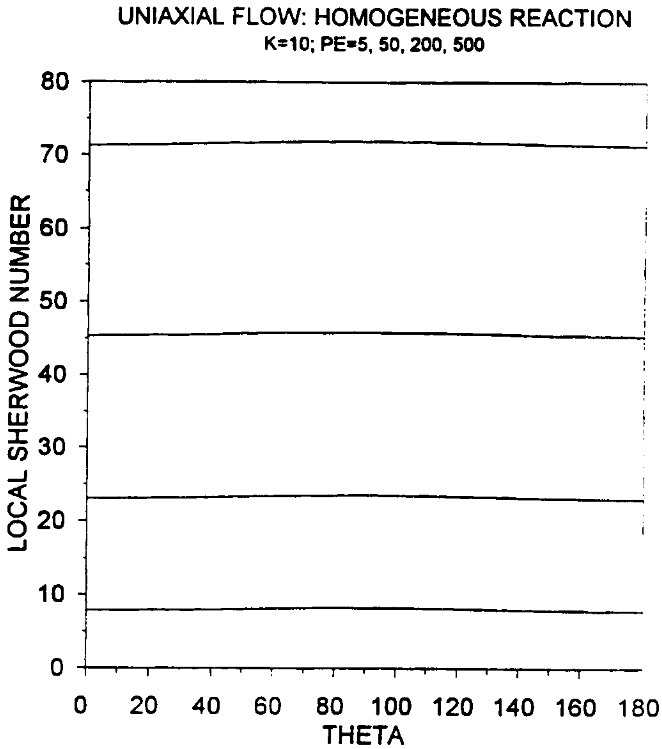

TABLE 1: Average Sherwood Numbers for Biaxial Flow

Pe	K	R	Avg. Sherwood N	NI	NM	NF	NE	N	TOL
5	0	10	2.4222332546	60	600	166	142	70	1E-06
5	1	10	3.4844020321	60	600	135	142	70	1E-06
5	2	10	4.2826214867	60	600	135	142	70	1E-06
5	5	10	6.0326632737	60	600	104	142	70	1E-06
5	10	10	8.0806645862	60	600	101	142	70	1E-06
50	5	5	16.8417150406	100	875	140	142	70	1E-06
50	10	5	23.3676877824	100	875	130	142	70	1E-06
200	5	5	32.6445658252	100	875	219	142	70	1E-06
200	10	5	45.7258627584	100	875	235	142	70	1E-06
500	5	5	51.0160617125	100	875	425	142	70	1E-06
500	10	5	71.7138264523	100	875	202	142	70	1E-06

TABLE 2: Average Sherwood Numbers for Uniaxial Flow

Pe	K	R	Avg. Sherwood N	NI	NM	NF	NE	N	TOL
5	0	10	2.6345022231	60	600	141	142	70	1E-06
5	1	10	3.5533852471	60	600	178	142	70	1E-06
5	2	10	4.3116939874	60	600	189	142	70	1E-06
5	5	10	6.0374513084	60	600	154	142	70	1E-06
5	10	10	8.0814290608	60	600	141	142	70	1E-06
50	5	5	16.8450206823	100	875	309	142	70	1E-06
50	10	5	23.3680425224	100	875	243	142	70	1E-06
200	5	5	32.6462378512	100	875	527	142	70	1E-06
200	10	5	45.7260072732	100	875	353	142	70	1E-06
500	10	5	71.7138969816	100	875	417	142	70	1E-06

NI Number of initial grid points, including the endpoints (NINIT)
NM Maximum number of grid points allowed (MXGRID)
NF Number of final grid points, including the endpoints (NFINAL)
NE Number of (first order) differential equations (NEQNS)
N Number of terms in the eigenfunction expansion
TOL Relative error control parameter